JOURNAL OF MODERN OPTICS, 20 JANUARY–15 FEBRUARY 2005
VOL. 52, NO. 2–3, 321–340

Taylor & Francis
Taylor & Francis Group

Second-order autocorrelation measurements of attosecond XUV pulse trains

P. TZALLAS†, D. CHARALAMBIDIS‡,
N. A. PAPADOGIANNIS‡, K. WITTE†
and G. D. TSAKIRIS†

†Max-Planck-Institut für Quantenoptik, D-85748 Garching, Germany
‡Foundation for Research and Technology—Hellas, Institute of Electronic Structure & Laser, PO Box 1527, GR-711 10 Heraklion, Crete, Greece and Department of Physics, University of Crete, PO Box 2208, GR-71003 Voutes-Heraklion, Crete, Greece

(*Received 9 June 2004; revised version 30 July 2004*)

Abstract. The unequivocal demonstration of attosecond XUV pulse train generation based on the synthesis of a comb of harmonics of an infrared femtosecond laser pulse is inevitably linked to a reliable method of pulse characterization in this temporal regime. The most commonly used method to date relies on a cross-correlation technique between the fundamental laser frequency and the XUV light from which a measurement of the relative phases of the consecutive harmonics is obtained and the attosecond temporal structure in a train of XUV pulses is inferred. Here we report on an alternative method that renders possible the direct observation of a train of attosecond pulses in form of a second-order autocorrelation trace. The method is an extension in the XUV spectral range of the well-established technique commonly used for the characterization of femtosecond laser pulses. Besides being the first direct visualization of a periodic attosecond structure, the approach supplies quantitative information on the overall pulse duration including the influence of the macroscopic conditions of generation.

1. Introduction

According to the superposition principle in wave mechanics, spatial or temporal energy localization comes about whenever mutually coherent waves are superimposed in time and space [1]. It is the interplay between constructive and destructive interference in a superposition of monochromatic light waves of equally spaced frequencies which manifest themselves in temporal beating, the underpinning process of short pulse generation. The mathematical description of wave superposition, Fourier synthesis, indicates that the larger the number of properly phased spectral components of comparable amplitudes, the more pronounced is the confinement in time. In this context, the extreme ultrviolet (XUV) harmonic emission from atoms of rare gases appears to be a most suitable candidate for the temporal localization of light to unprecedented short time scales [2, 3].

Journal of Modern Optics ISSN 0950–0340 print/ISSN 1362–3044 online © 2005 Taylor & Francis Ltd
http://www.tandf.co.uk/journals
DOI: 10.1080/09500340412331301533

In the quest for the generation of attosecond pulses two main and distinct approaches are being presently pursued, both based on the harmonic emission from atoms. The first approach employs many-cycle laser pulses and aims at the production of a train of attosecond XUV pulses [4–7]. The second approach uses few-cycle laser pulses and its goal is the direct generation of isolated attosecond XUV pulses [8–12]. In the interaction of low frequency intense laser pulses with atoms, the atomic potential is depressed by the electric field of the pulse so that a bound electron can tunnel through the potential barrier thus formed. Subsequently, the electron moves in the continuum while it gains energy under the influence of the external laser field. Those electrons that return to the vicinity of the parent ion, may recombine to emit photons with energy $\hbar\omega = I_p + E_k$, where I_p is the ionization potential of the atom and E_k is the kinetic energy that the electron gained during its excursion in the continuum. This well-known semi-classical model [13] provides a very satisfactory picture of the physical process of harmonic generation in atoms. The energy that the electron can gain and the corresponding trajectory in the continuum depend sensitively on the intensity of the field and its phase at the time of ionization. For reasons of symmetry, the periodic motion of the electron gives rise to a spectrum consisting only of a series of equally spaced peaks around the frequencies of the odd harmonic of the laser field frequency. According to both the semi-classical description [13] and its extension to a full quantum theory [14] of the interaction of an intense low frequency laser pulse with atoms, the frequency spectrum of the generated harmonics is determined by the evolution of specific electron trajectories in the continuum. Further, the harmonic spectrum exhibits two characteristic regions relevant to the two approaches of attosecond pulse generation, namely the 'cut-off region' and the 'plateau region'. The 'cut-off' region corresponds to the highest energy with which the electron may recombine following one specific trajectory. In this region the emitted photon intensity drops rapidly at energies higher than the cut-off energy given by $\hbar\omega_{max} = I_p + 3.17U_p$, where $U_p = e^2E_L/4m\omega_L^2$ is the average (ponderomotive) energy of the free electron in the laser electric field. The 'plateau' spectral region at photon energies below $\hbar\omega_{max}$ consists of a frequency 'comb' of approximately equal intensity peaks at twice the laser field frequency. The near to cut-off spectral region is used for isolated attosecond pulse generation. Few-cycle laser pulses [15–19] are used, so that the emission ensues only during a small fraction of the optical cycle and by the cycle with the highest amplitude within the optical pulse. Under these circumstances, there is a single electron trajectory contributing to the harmonic emission [9]. Using appropriate filters, the quasi-continuous spectral distribution of the cut-off comprising highly energetic XUV radiation is separated and isolated pulses with sub-femtosecond pulse duration are produced [10–12]. These isolated pulses have been already used for a pump–probe experiment in an ultra fast time domain spectroscopy application [20]. A crucial parameter in this generation mechanism is the relative phase between the carrier frequency and the envelope of the few-cycle pulse [21] that determines the location of the highest amplitude cycle under the pulse envelope. The reproducibility of the emission characteristics relies sensitively on the stabilization of this relative phase; a task that has already been achieved [22] and more recently also in amplified few-cycle pulses [23].

In contrast, when laser pulses comprising many cycles are used, the harmonic emission occurs over many cycles within the laser pulse envelope. In this case, a

number of electronic wave packets are unleashed into the continuum following different trajectories. Theoretical work has shown that from all the interfering quantum paths two trajectories prevail contributing to a given photon energy below the cut-off [24]. Both of them have return times less than a laser period, but one is almost twice as long as the other so one speaks of a 'long' and a 'short' trajectory. As far as the attosecond pulse generation is concerned, it is the relative phase between consecutive harmonics that plays a decisive role. Only when the phases of the harmonics in the frequency comb are 'locked', i.e. if the phase difference between all the neighbouring harmonics is common and constant at any given time in the pulse, Fourier-transform-limited (FTL) spikes of attosecond duration would appear in the time-domain as a result of frequency beating. To that effect, the 'short' trajectory displays less total phase accumulation during the excursion in the continuum and thus it contributes more significantly to the formation of temporal spikes. According to simulations in which the propagation through the medium is taken into account, only the 'short' trajectory survives [24]. This is a fortuitous effect ultimately leading to a well-defined train of attosecond pulses emerging from the interaction volume. Nonetheless, experiments indicate that this 'cleansing' effect appears to occur only at the central part of the harmonic beam [25].

In the pursuit for the generation of attosecond pulses, both the many- and the few-cycle pulse routes presently are being vigorously pursued [4–12]. Although attosecond structures have been previously reported, due to lack of nonlinear XUV autocorrelators, all methods used so far for their investigation [4–6, 10–12] are based on sophisticated cross-correlation approaches with the fundamental laser field. While they have decisively contributed to the development of attoscience in its early stage, the interpretation of the data and their use in extracting quantitative results inevitably requires modelling based on appropriate approximations and/or use of theoretically calculated parameters. The recent debut of attosecond pulses in pump–probe applications [20] also relies on such cross-correlation techniques. In this case, the accuracy with which the laser field is known and that of the model used determine the temporal resolution of the technique. As attoscience is maturing, direct high-resolution time-domain metrology approaches become of paramount importance.

In this report we give a comprehensive account of the work we have performed on gaining access to attosecond time-scales and observe ultra fast processes in this temporal regime. A brief account of this work has already been communicated in [7, 26]. Our approach is based on nonlinearly autocorrelating attosecond XUV radiation through its interaction with an atomic system and it thus represents a non-trivial extension of a well-established approach for many years successfully used in optical femtosecond metrology. Short wavelength second-order autocorrelation has been previously limited in measuring the duration of individual XUV [27, 28] or UV [29] harmonics in the temporal regime of a few tens of femtoseconds. The present work is pivotal in expanding the applicability of this nonlinear technique to the broadband radiation of a coherent superposition of harmonics and thus to the attosecond regime. While the unique capabilities of the new approach are demonstrated here in performing the first direct pulse duration measurement of the individual 'wagons' of an attosecond pulse train, the method itself initiates the XUV pump–XUV probe studies in sub-femtosecond scale dynamics. In principle, it is a model-independent method that provides a direct

temporal resolution of the order of the width of the attosecond wavepacket. Apart from its importance to the characterization, optimization and time-domain applications of harmonic attosecond fields, the method becomes highly pertinent in connection with novel nonlinear pump–probe experiments using the up-coming XUV free electron laser sources which have recently opened up a new and exciting field of nonlinear physics [30].

2. The methodology

The mapping of phase-amplitude distributions of an ultra-short pulse or an ultra-fast process relies on a nonlinear process. Thus, in the well-established femtosecond metrology, the most widely used methods rely on a nonlinear effect induced solely by the radiation to be characterized. Already a second-order autocorrelation (AC) is sensitive to the spectral phase distribution of the radiation to be analysed. In pico- and femtosecond laser laboratories, the pulse duration has been for many years routinely extracted to a satisfactory degree of accuracy from a measurement of the second-order AC trace.

The extension of the approach to sub-femtosecond XUV pulses poses several formidable problems since attosecond pulses are: (a) spectrally much broader and in the UV–XUV spectral range marked by a complete lack of refractive optical components and even reflective optics is either of low reflectance or narrow bandwidth and (b) orders of magnitude weaker, thus requiring ultra-sensitive nonlinear detectors with a flat broadband response. In the present work, we report a direct measurement that surmounts these obstacles. The key factors to this progress have been (i) the technique of the dispersionless volume autocorrelation and (ii) the demonstration of the two-photon non-resonant ionization process in helium as an appropriate flat response detector [31]. The experimental results [7] bear direct evidence that a synthesis of five harmonics results in the formation of a train of XUV pulses each one having a duration of $\sim$780 as.

3. Apparatus for the XUV second-order autocorrelation measurements

In the present experiment, the 10 Hz Ti:sapphire laser system at Max-Planck-Institut für Quantenoptik, ATLAS II, delivering 130 fs pulses, with energy up to 300 mJ and carrier wavelength at 790 nm, was used. A schematic of the experimental set-up is shown in figure 1.

The annular-shaped [32] input laser beam, with 2 cm outer diameter and about $\sim$10 mJ energy, is focused with a 1.5 m lens into a piezoelectrically pulsed xenon gas jet (N–Xe) where the harmonic generation takes place. The annular input laser beam was employed at higher laser intensities to reduce the amount of infrared light (IR) reaching the filter. The laser intensity at the Xe gas jet is estimated to be in the range of 5×10^{13} to 1×10^{14} W cm^{-2}, which is below the saturation intensity value of about 3×10^{14} W cm^{-2} for Xe^{+}. The laser beam focus was placed $\sim$6 mm before the Xe gas jet, at a position for which theoretical calculations predict optimum spatial and temporal harmonic phase locking [33]. For the laser intensities used, harmonics of up to the 15th are produced. An aperture is placed after the Xe gas jet position in order to block the annular part of the fundamental laser beam, while it leaves the central part, which contains the harmonic beam, to pass through. Directly after it, a 0.2 μm indium filter, positioned at a distance of $\sim$1 m

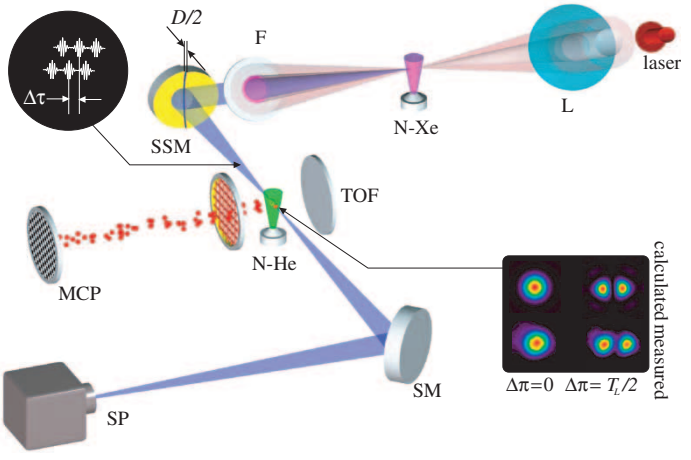

Figure 1. Schematic of the experimental set-up of the second-order XUV volume autocorrelator. The laser beam is focused by the lens (L) into a Xe nozzle (N-Xe) where up to the 15th harmonic of the laser frequency is generated. The 7th to 15th harmonics are selected by the indium filter (F) and enter the volume autocorrelator. Instead of a beam splitter, the second-order XUV autocorrelator consists of a split spherical mirror (SSP) serving as a focusing wave-front divider. The XUV pulse train is split into two replicas as shown in the upper left inset. The autocorrelator delay is introduced by the relative motion of the two halves of the mirror. As a nonlinear detector a two-photon ionized He gas (N-He) is used, and the He ion yield, analysed by a time-of-flight mass spectrometer (TOF), and recorded by a micro-channel plane detector (MCP), provides the AC signal. The lower right inset shows, for zero and $T_L/2$ delay ($D = \lambda/2$ displacement), T_L being the period of the laser, the calculated and measured cross-sectional laser intensity distribution at the focal plane.

from the Xe gas jet, selects a group of harmonics from the 7th to the 15th and blocks the fundamental part of the beam. A wavefront splitting arrangement [34–36] consisting of a gold spherical mirror (SSM) with 30 cm radius of curvature cut into two halves (see figure 1) was used to focus the harmonic radiation. One of these halves is mounted on a piezo-crystal translation unit and its positioning can be controlled with a resolution of ~6 nm over a total travel of ~12 μm. The two parts of the bisected XUV pulse train (see inset in figure 1) are brought into a common focus in a second gas jet produced by a nozzle (N-He) of the same type as the first, but filled with helium at a backing pressure of ~2 atm. This gas jet has an orifice of 1 mm diameter and was equipped with a flow collimator tip 15 mm long with 1 mm inner diameter. The XUV beam focus was located at 2 mm below the collimator tip in order to have high atomic density at the interaction region. Having the same type of gas jet (Lasertechnics LPV) as the one characterized in detail in [37], we can estimate that the atomic density at the interaction region is $\sim 10^{16}$ atoms cm^{-3}. The ionization products are analysed by a ~50 cm long time-of-flight (TOF) mass spectrometer and detected by a micro-channel plate (MCP) detector. The collimator of the He gas jet is placed almost at the centre of the TOF accelerating region, and it is connected to a voltage supply that allows adjustment of its potential so that the extraction field in the acceleration region remains homogeneous. The harmonic radiation was monitored by a XUV spectrometer (SP) coupled to the harmonic radiation through a gold-coated spherical mirror (SM) with 60 cm radius of curvature. The spectrometer was operated with narrow

entrance and exit slits in order to measure the spectral bandwidth of the harmonics. For the second-order AC, the ionization products are detected as a function of the delay $\Delta\tau$ corresponding to a total displacement D (twice the actual separation) between the two half mirrors. The focal spot produced by the split mirror exhibits an intricate pattern as a function of the relative displacement, but at a displacement of multiples of $\lambda/2$ the well-known Airy pattern is divided into two equal spots, each one having about half the maximum intensity. The pattern has been calculated for the fundamental frequency and it is shown for two displacements in the lower inset of figure 1 along with the measured one using the fundamental laser frequency. The double spot shape is used prior to an experimental run to adjust the orientation of the movable half of the mirror and position the fine travel of 12 μm in the middle of the 40 μm extent of the laser pulse where the intensity is maximum. In addition, it provides the means of positioning the laser beam centrally within the spherical mirror aperture by adjusting the two spots to exhibit the same brightness. This ensures a 50% splitting of the incident laser beam.

4. The characterization of the harmonic comb

In figure 2 (*a*), the recorded harmonic spectrum is shown before and after the In filter. The spectral width of the harmonics was found to be close to the resolution of the spectrometer which in this spectral region is ~1 nm and the In filter transmission was measured to be 20% at 88 nm (9th harmonic). The relative intensity amplitudes of the harmonics after the corrections of the reflectivity of the gold mirror and the efficiency of the spectrograph and detector were 7th:9th:11th:13th:15th → 0.32:1.0:0.30:0.11:0.01. Under these experimental conditions the total harmonic energy after the reflection from the split gold mirror is estimated to be ~5 nJ [38]. The synthesis of these five harmonics between the 7th and 15th is the object of our characterization. Using the knife-edge technique at far field [39], we found that the spatial profiles of the harmonics (figure 2 (*b*)) are close to Gaussian with divergence (half-angle) $\Theta \sim 1.6$ mrad for the 7th and $\Theta \sim 1.3$ mrad for all other harmonics at the $1/e^2$ of the beam intensity. As a result, the XUV beam diameter on the split mirror is $D_{\mathrm{XUV}} \approx 4.0$ mm. Given that the laser beam is about two times diffraction limited and assuming an effective order of nonlinearity for the harmonics of $p \sim 6$ [40], one obtains a spot size at the generating nonlinear medium of $2w^0_{\mathrm{XUV}} \approx 60$ μm and using the measured divergence, an average $M^2 \approx 1.7$ factor for the harmonics in the superposition. Using this value for the M^2, the diameter of the focal spot of the XUV radiation produced by the split mirror at the He jet is estimated to be $2w_{\mathrm{XUV}} \approx 8$ μm. This is close to the directly measured value of 10 μm for the spot size of the 13th and 15th harmonic generated and focused under very similar experimental conditions [39].

Despite the small number of harmonics and the unequal amplitudes between them, an ideal phase-locking of the harmonics (all phase differences equal to zero) would produce an attosecond train with full-width-half-maximum (FWHM) 'wagon' duration of $\tau_{\mathrm{XUV}} = 315$ as. This is depicted in figure 3 (*b*) where the resulting field and intensity of the individual 'wagons' for the experimentally measured harmonic intensity amplitudes are shown. It is interesting to note that for equal harmonic intensity amplitude, the corresponding 'wagon' duration would

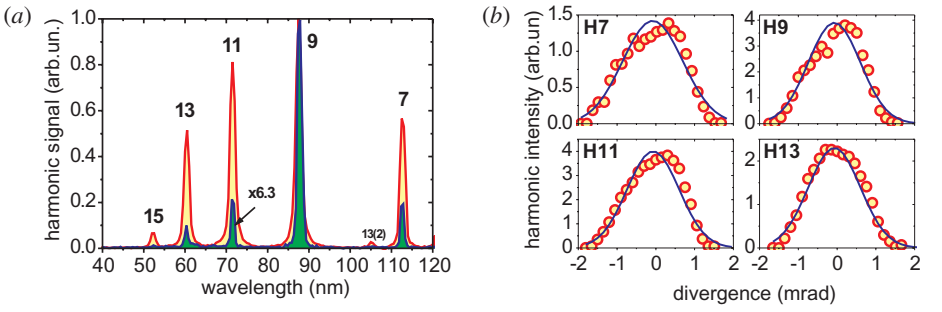

Figure 2. The harmonic 'comb'. (*a*) The higher order harmonic generation spectra produced in the Xe jet. The red-line yellow-shaded spectrum corresponds to the harmonics as measured without the In filter and the blue-line green-shaded to the one transmitted through the In filter. Both spectra are normalized to unity. The relative intensity amplitude of the harmonics after the corrections for the reflectivity of the gold mirror and the efficiency of the spectrograph and detector is 0.32(7th):1.0(9th):0.30(11th):0.11(13th):0.01(15th). (*b*) The spatial profile of the 7th, 9th, 11th and 13th harmonic. For all harmonics the beam profile was very close to Gaussian while the divergence was found to be ~1.6 mrad for 7th and ~1.3 mrad for 9th–13th at $1/e^2$ of the harmonic intensity. In all diagrams, the zero of the divergence axis is arbitrarily chosen.

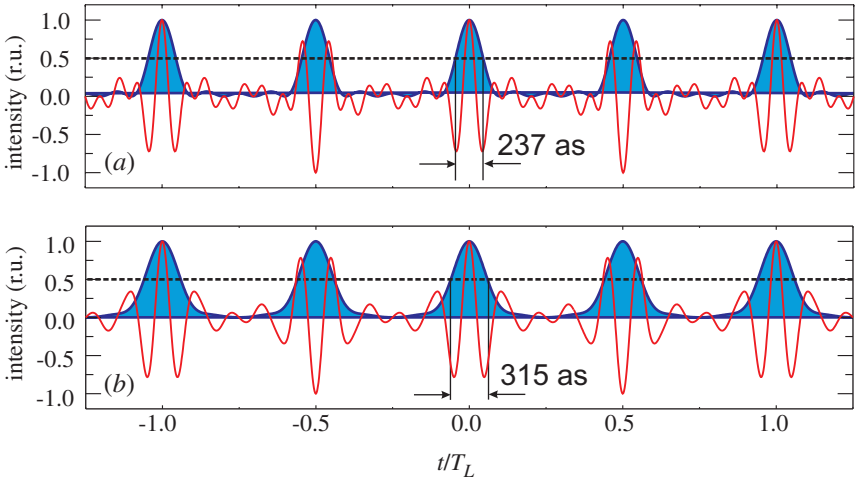

Figure 3. The electric field amplitude (red line) and the intensity (blue-shaded line) of a comb of five odd harmonics (7th to 15th) for two cases. For (*a*) equal intensity ratios and (*b*) with relative intensity ratios of 0.32(7th):1.0(9th):0.30(11th):0.11(13th): 0.01(15th). Assuming for both cases zero initial phases for all the harmonics (Fourier transform limited pulses), the duration of each 'wagon' in case (*a*) is 237 as whereas for the experimentally measured intensity ratio it is 315 as.

be 237 as (see figure 3 (*a*)). This is reasonably close to the theoretical value for the FTL case $\tau_{\mathrm{XUV}} \approx T_{\mathrm{L}}/2N = 263$ as for the duration of each sub-cycle pulse resulting from the synthesis of $N = 5$ equal amplitude harmonics of the laser field with period T_{L}. It appears that the influence of unequal harmonic intensities on the duration of the individual pulses in the train is rather weak.

5. The nonlinear detector

The combination of He as an ionization medium and In as a filter material for the selection of a group of harmonics is a judicious choice presenting several advantages. This becomes clear if one considers the possible ionization channels due to the available photon energies in relation to the ionization potential (IP) of 24.6 eV for He. These channels are schematically shown in figure 4. On the high frequency side, only harmonics higher than the 15th (17th, 19th, ...) can give rise to single photon ionization. As can be seen in figure 2 (*a*) where the transmitted spectrum through the 0.2 μm In filter is shown, there is no measurable signal corresponding to the 17th harmonic at 46.5 nm. On the low frequency side, the 7th harmonic is transmitted, but all lower harmonics are practically filtered out. Moreover, all harmonics below the 9th can only induce in the non-mixing combination three-photon ionization with yields of many orders of magnitude less than that of the two-photon ionization process. The harmonics in the superposition used can only induce *two-photon ionization*, either by two photons of the same energy (with the exemption of the 7th harmonic) or by any combination of the photon energies in the superposition (see figure 4).

The properties of this nonlinear detector have been investigated in detail in a previous experiment and the yields for the same harmonic superposition calculated from the time-dependent Schrödinger equation for He in a polychromatic laser field [31]. These calculations have revealed a relatively flat detector response for the harmonics used. Moreover, as shown in figure 3, any fluctuation in the yield of each individual harmonic has very small influence on the electric field of the harmonic superposition. In order to asses whether the 17th harmonic is sufficiently suppressed so as not to cause single photon ionization, we have performed measurements with the present experimental set-up of the ion yield versus harmonic intensity for three ions (He^+, H_2O^+ and Xe^+). Figure 5 (*a*) shows a typical TOF mass spectrum produced by the harmonic superposition at two different XUV intensities having a ratio of two. As can be seen, the He^+ peak increases four times while the rest of the peaks simply double. The three graphs in figure 5 (*b*) give the ion yield variation as a function of the 9th and 11th harmonic intensity

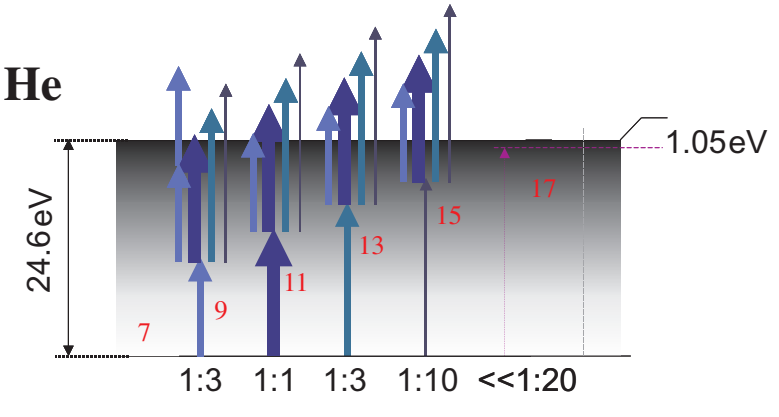

Figure 4. Schematic diagram of the ionization process by the harmonic comb. The ionization of helium occurs primarily through two-XUV-photon non-resonant absorption from all possible combinations of the 7th to 15th harmonic.

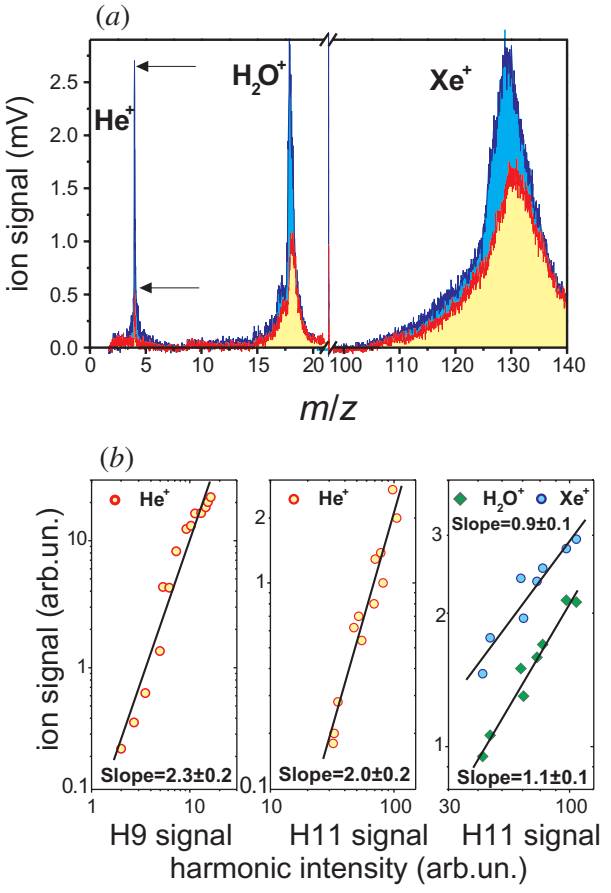

Figure 5. Characterization of the nonlinear detector. (*a*) The measured XUV time-of-flight mass spectrum for two different harmonic intensities. In the time-of-flight spectrum, two of the mass peaks can be assigned to single photon ionization of H_2O and Xe and one to the two-photon ionization of the He atoms. The blue-cyan shaded spectrum corresponds to a harmonic intensity twice as high as the one which is red-yellow shaded. (*b*) The XUV intensity dependences of some of the masses. In log–log scale the slope of the He ion yield as a function of the intensity of the 9th harmonic and the 11th harmonic is 2.3 ± 0.2 and 2.0 ± 0.2, respectively. In contrast, the slope of the ion yield dependence on the intensity of the 11th harmonic for H_2O and Xe is found to be 0.9 ± 0.1 and 1.1 ± 0.1, respectively.

for the He^+ ions and of the 11th harmonic for H_2O^+ and Xe^+ ions. The fact that the intensity dependence for He^+ (IP = 24.6 eV) is very nearly quadratic while for H_2O^+ (IP = 12.6 eV) and Xe^+ (IP = 12.1 eV) it is linear, provides clear evidence that the influence of the 17th harmonic is negligible and that the He^+ ionization signal is due to two-photon absorption and thus ideally suited for a second-order AC measurement.

Additionally, assuming a pulse duration of $\tau_q = \tau_L/p^{1/2} = 50$ fs for the qth harmonic (with $p = 6$) and taking into account that the XUV spot diameter at the focus is $\sim$10 μm, we can estimate the intensity at the interaction region as $\sim 10^{11}$ W cm^{-2}. Using the known He two-photon absorption cross-section [31],

the calculated ion yield is consistent with the observed number of $\sim$90 ions pulse^{-1}.

6. The volume autocorrelation technique

A thorough understanding of the volume AC technique is necessary in order to be able to extract from the ionization AC trace the duration of the individual 'wagons' in the attosecond pulse train. The detected signal is due to two-photon ionization of the helium gas resulting from the coherent superposition of the two split parts of the attosecond train (see upper left inset in figure 1). Assuming that the generated XUV radiation possesses cylindrical symmetry, it represents a second-order autocorrelation. There are two points that distinguish this technique from the conventional Michelson interferometer based on a nonlinear crystal or a nonlinear photodiode. (a) The signal produced emanates from the interaction of the XUV pulse with the He atoms within a volume defined by the focusing properties of the spherical mirror and not from a plane as in the case of a nonlinear crystal. (b) Unlike the amplitude splitting arrangements, the split mirror technique is a wavefront splitting device and as such, a delay variation results not in a change of the energy reaching the detector, but simply in spatial redistribution of the energy in the focal volume according to the diffraction principle.

For a given wavelength, a displacement of $D = \lambda/2$ (delay $\Delta\tau = T_{\mathrm{L}}/2$) between the two half mirrors has the effect of dividing the focal spot for zero displacement (Airy spot) with peak intensity $I_{\max}$ into two having approximately the same size as the original (see lower right inset of figure 1). Since the total energy in the interaction volume remains constant and independent of the relative delay, the splitting of the focal spot into two means that the maximum light intensity in each one of them is $I \approx I_{\max}/2$. If the detector were linear, the signal S in both cases would be $S_{D=0} \propto I_{\max} \approx S_{D=\lambda/2} \propto 2(I_{\max}/2)$, i.e. no modulation of the signal with the relative delay would be observed. If instead a nonlinear detector were used, the rearrangement of the local intensity inside the interaction volume according to diffraction would produce a modulation in the measured signal.

This is because for a quadratic detector like the two-photon ionization process in helium the corresponding response would be: $S_{D=0} \propto I_{\max}^2 \neq S_{D=\lambda/2} \propto 2(I_{\max}/2)^2$. For the quantitative analysis of the signal, a more accurate estimation of the signal evolution with the delay is necessary. As an example, we consider the harmonic superposition consisting of four harmonics with equal amplitude (7th, 9th, 11th and 13th). For this harmonic 'comb', we have calculated for various displacements between the two mirror halves the time-averaged field distribution $E(D, x, y, z) = \sum_{n=7}^{13} E_n(D, x, y, z)$ at the focal spot of our spherical mirror. The intensity distribution $I(D, x, y, z) = E(D, x, y, z)E^*(D, x, y, z)$ for six particular values of the displacement perpendicular and parallel to the propagation direction are shown in figure 6 in the form of colour contour plots. As is schematically shown at the top inset of figure 6, the ionization signal seen by the TOF detector is due to the total contribution from the entire interaction volume ΔV, therefore, for a given displacement this would be $S(D) \propto \int\int\int_{\Delta V} I^2(D, x, y, z)\,\mathrm{d}x\,\mathrm{d}y\,\mathrm{d}z$.

The result of this numerical simulation is depicted in figure 7. The points are the results of the numerical integration of the square of the intensity distribution over a box with transverse sides six times the Airy spot radius and length six times the Rayleigh range of the focusing mirror for discrete values of the

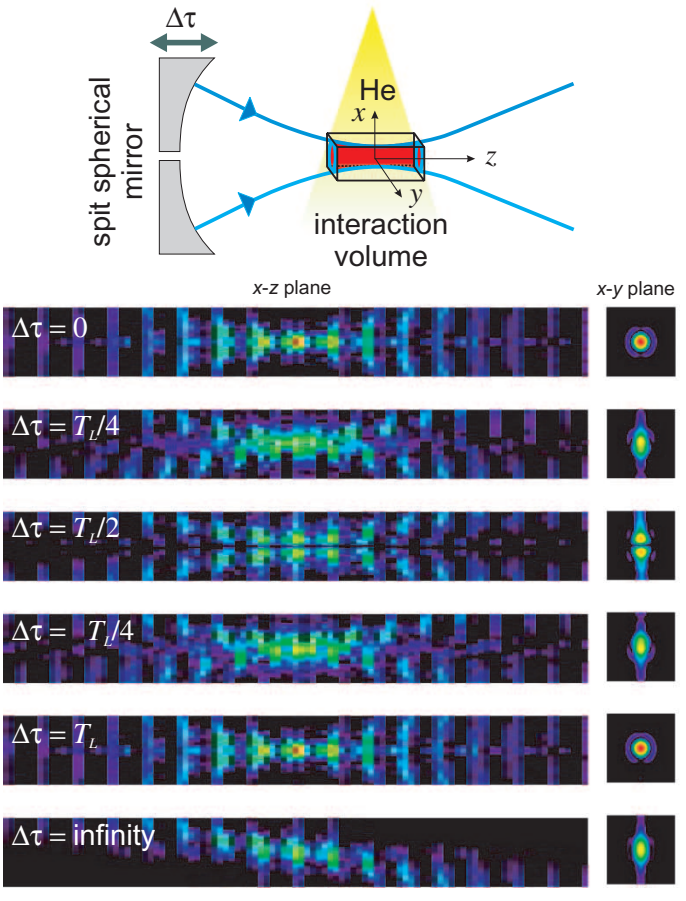

Figure 6. Three-dimensional colour contours depicting in logarithmic scale over three decades the calculated intensity distribution at the interaction region of the volume autocorrelator for the indicated delays corresponding to a given mirror displacement. In the x–y plane, the Airy spot for zero delay becomes a double maximum distribution for $T_{\mathrm{L}}/2$ delay corresponding to $D = \lambda/2$ displacement (T_{L} is the period of the laser).

displacement D. The smooth red curve through the points represents the interferometric equivalent of the volume autocorrelation for the superposition of the four harmonics. The delay $\Delta\tau$ in periods of the fundamental frequency T_{L} corresponds to the overall displacement D between the two half mirrors. We have compared these results to those obtained from a hypothetical collinear (conventional) interferometric autocorrelation given by the expression $S(\tau) = \int_{-\infty}^{+\infty} |[E_{\mathrm{T}}(t) + E_{\mathrm{T}}(t-\tau)]^2|^2 \, \mathrm{d}t$, where E_{T} is the total electric field of the same harmonic superposition of plane waves having equal amplitudes and ideal phase locking. The volume AC trace exhibits exactly the same structure (compare solid red and blue curve in figure 7), but due to coarse sampling used in the calculation (open circle points), not all the peaks within a period are visible (there should be 13 oscillations corresponding to the highest frequency in the superposition). The background level is two times the contribution of only one half of the mirror. The corresponding intensity distribution in this case is the last panel in

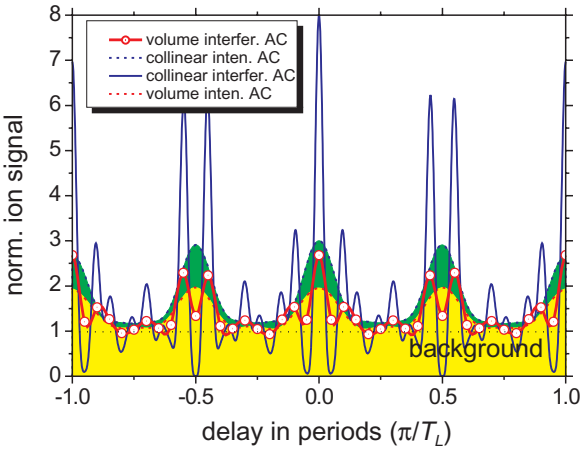

Figure 7. Comparison of the interferometric and intensity autocorrelation traces for the case of a collinear and a volume autocorrelator. For both cases the total field is that corresponding to the superposition of the 7th to the 15th harmonics with equal amplitudes.

figure 6 for $\Delta\tau = \infty$. The main difference compared to the conventional interferometric AC trace is the peak-to-background ratio, which instead of 8:1 is only ~2.75:1 for the volume AC.

The corresponding intensity autocorrelation is obtained from the interferometric by cycle-averaging the fast oscillations (dashed red yellow shaded and dashed blue green shaded lines in the same graph of figure 7). Again, we observe a reduction of the peak to background ratio from 3:1 (conventional) to ~2:1 (volume). It becomes apparent that although the contrast of the signal is reduced, still it should be possible to observe modulation with the delay using the volume AC technique.

7. Direct measurement of trains of attosecond XUV pulses

The results of the first genuine second-order autocorrelation measurement of a train of XUV pulses offering direct observation of attosecond temporal light confinement are summarized in figures 8 and 9.

In particular, figure 8 gives the results of a scan over ~130 fs in which the ion signal due to two-photon ionization of He and that due to single photon ionization of Xe as a function of a coarse variation of the delay Δt is plotted. These results represent a further confirmation that the He gas acts as a two-photon detector for the XUV radiation in the harmonic superposition. Whereas the He signal exhibits a modulation according to the degree of overlapping of the two XUV pulses (see figure 1), the signal corresponding to singly ionized Xe stays constant. From the He results we deduce an overall duration for the XUV macro-pulse comprising the harmonic superposition in frequency and the pulse train in time. The solid line in figure 8 shows the best fit of a Gaussian pulse to the measured He data. The measured peak-to-background ratio is close to 2 in accordance to our numerical simulations for the intensity AC of the volume autocorrelator. The resulting full width at half maximum (FWHM)

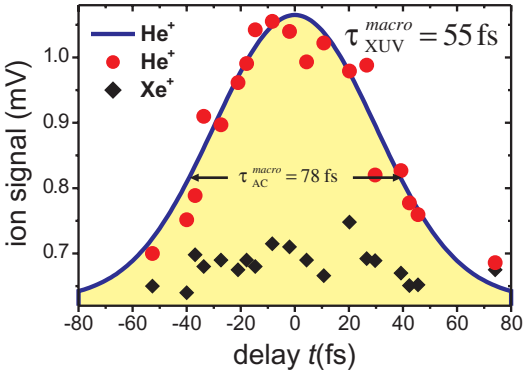

Figure 8. Measured autocorrelation traces of the total XUV pulse resulting from the superposition of the 7th to 15th harmonics. The circles correspond to the He^+ while the rhombi to the Xe^+ signal.

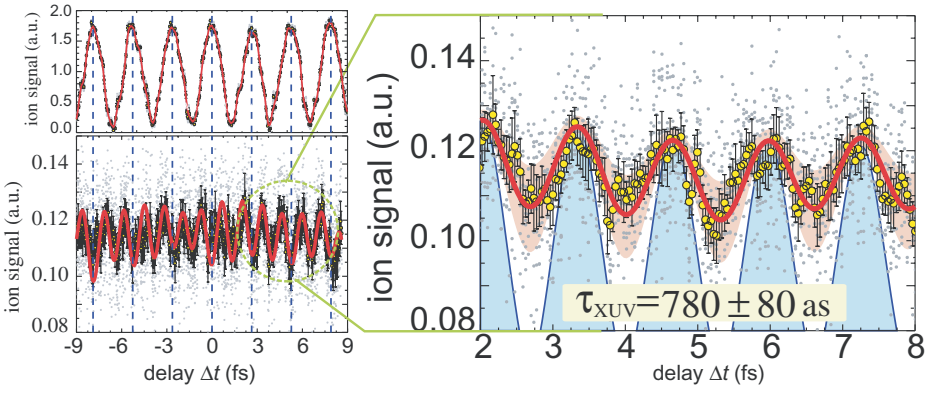

Figure 9. Measured nonlinear volume AC traces. The upper trace in the left panel is the higher-order AC trace of the fundamental laser field. For this acquisition, the harmonic generation was turned off and the In filter was removed. The period of the observed oscillation is equal to the laser period, i.e. 2.63 fs. The trace at the bottom of the left panel is a measured ~18 fs long second-order volume intensity AC trace of the superposition of the five harmonics 7th–15th while the trace to the right is a blow-up of the green-shaded region covering a delay range of about 3 laser cycles. The grey points are the measured data (10 points are accumulated per each position). The yellow points are their average and the error bars shown correspond to one standard deviation. A clear modulation with half the laser period is observable in the entire trace. The red curve is the best fit of an analytical function given by the sum of a sequence of Gaussian distributions. The common temporal width τ_{AC} of the distributions is the fit parameter, with a best value being 1.1 fs, which corresponds to a duration of $\tau_{XUV} = 780$ as for each XUV pulse in the train. The blue lines in the expanded area are the individual (not superimposed) Gaussian distributions. As the shaded area indicates, the scatter in the experimental points give an estimate for the individual 'wagon' duration in the XUV synthesis of the five harmonics as $\tau_{XUV} = 780 \pm 80$ as.

of the AC trace is $\tau_{AC}^{macro} = 78 \pm 7$ fs and thus using the well-known formula for Gaussian pulses, the duration of the envelope of the macro-pulse encompassing the individual 'wagons' in the train is $\tau_{XUV}^{macro} = \tau_{AC}^{macro}/2^{1/2} \approx 55$ fs. Compared to the values predicted by the lowest-order perturbation theory (LOPT) for the

130 fs long harmonic generating laser pulses, this value is 12–64% larger than the values for the different harmonics of the superposition and approximately 27% larger than the value for the most intense harmonic (9th harmonic). This is compatible with the well-known lower-order nonlinearity of the harmonic generation process compared to the order of the process obtained by means of multiphoton LOPT.

The attosecond structure becomes visible when a fine scan in the delay is performed. This is illustrated in the graphs of figure 9 where the traces of the ion signal, for a total temporal overlap of ~18 fs near the peak of the laser pulse and as a consequence of the XUV macro-pulse in steps of ~37 as, are shown. For each position of the piezo-crystal, ~10 data points were accumulated (grey dots). To reduce the fluctuations in the signal, the running average over 15 data points for the ion yield and the corresponding standard deviation were calculated (yellow point with errors bars). This has, as a consequence, an increase of the delay step to 56 as, but also the unveiling of an important feature in the signal that provides the evidence for an attosecond pulse train. In particular, in the lower left panel of figure 9 and in the magnification in the right panel, a distinct modulation comprising two peaks within an optical cycle of the fundamental frequency is clearly perceived. The double peak per laser period is the result of having a frequency comb with twice the laser frequency between successive peaks. A reliable *in situ* calibration of the optical period is afforded by recording the signal due to multi-photon ionization of He using laser light. This higher-order AC trace is shown in the upper left panel of figure 9 and it is acquired with the same experimental set-up, but with a solid laser beam instead of an annular one, without the In filter and with the Xe jet turned off. Theoretically, our micro-positioning device provides enough resolution to obtain the interferometric XUV trace. With a step size of 20 as (6 nm), about 14 points can be acquired within the period of the 9th harmonic, which is the most dominant. However, the shot-to-shot fluctuations inherent in the ionization signal do not allow this acquisition. The data averaging procedure we have used yields instead the equivalent of the intensity AC trace.

An average duration over all the 'wagons' in the train can be inferred from our AC data by extending the standard procedure employed in second-order AC measurements of single pulses and performing fitting of the sum of a sequence of Gaussian pulses with their common duration τ_{AC} as a single fit parameter. This tacitly assumes that the analytic representation of each of the attosecond pulses in the train also has the form of a Gaussian. This is common practice in second-order AC measurements, where a pulse form has always to be assumed in order to extract the pulse duration. The amplitudes for the individual XUV pulses are taken from the peaks in the AC data and the measured background level at ~50% of the signal (see also figure 8). The red curve in the lower left panel of figure 9 is the best fit obtained for $\tau_{AC} = 1.1$ fs. The average pulse duration of the 'wagon' in the attosecond train is thus $\tau_{XUV} = \tau_{AC}/2^{1/2} = 780$ as. In the magnified section in the right panel of figure 9, we have plotted, in addition to the best fit, the AC trace for $\tau_{XUV} = 700$ as and 860 as. The modulation is accordingly enhanced or reduced so that it encompasses the breadth of the scatter in the data points thus giving an estimate of $\tau_{XUV} = 780 \pm 80$ as for the average duration range of the attosecond peak.

8. Discussion and conclusions

Although the second-order autocorrelation technique provides a direct duration measurement, the result depends on the pulse shape assumed and in cases of complex pulse shapes as those encountered in this experiment, the task of a more rigorous deconvolution becomes rather formidable. Due to the limited region around zero delay covered by the scan we have performed, no information can be ascertained as to whether the individual 'wagons' have variable duration and/or spacing between them. Nevertheless, within the accuracy limitations of the second-order AC technique, the simple deconvolution procedure we have adopted here gives an average duration, which is more than double the FTL value.

The considerable deviation of the individual 'wagon' duration from its FTL value of $\tau_{\mathrm{XUV}}^{\mathrm{FTL}} = 315$ as (see figure 3) can be attributed to either systematic errors or to physical reasons. We have estimated the broadening effects of a number of possible systematic errors. For example due to: (a) deviation of the detector spectral response (He) from perfect flatness, (b) detector retardation effects due to virtual states being close to resonant lines of the He atom and (c) geometrical smearing effects [41] arising from the two non-collinear XUV beams emanating from the split mirror. In all cases the estimated error amounts to 5–10% of the FTL value and thus is inadequate for explaining the large deviation from the measured value.

This points to phase correlated spectral components but with imperfect phase locking of the harmonics. It has been recently indicated [6] that the harmonics generated in rare gases possess an inherent linear chirp due to a lack of synchronization during their generation process. Quantitatively, for a superposition of the harmonics this can be expressed as a quadratic dependence of the relative spectral phase on the harmonic frequency, i.e. for the qth harmonic the corresponding spectral phase is given by $\varphi(\omega_q) = \Delta t \omega_{\mathrm{L}}(q - q_0)^2/4$, where Δt is the temporal drift (harmonic chirp) between harmonics and q_0 is the first harmonic in the superposition. According to the results reported in [6], the harmonic chirp Δt depends on the rare gas and the laser intensity and for Xe and laser intensities 5×10^{13}–10^{14} W cm^{-2} (close to the intensities used in our experiments), Δt varies between 150 and 250 as. For our superposition of five harmonics generated in Xe, we have calculated the temporal structure of the XUV intensity for three values of Δt. The results are shown in the upper panel of figure 10. As can be seen, for higher harmonic chirp values the 'wagons' in the attosecond pulse train become broader and skew and for even higher values they acquire multiple peaks. For $\Delta t = 350$ as, we have calculated the corresponding autocorrelation trace and in the lower panel of figure 10 compared it to our experimental results. Within the accuracy of the experimental measurement, the agreement is excellent. However, the value of Δt used in this comparison is rather high and not compatible with the measured values of 150–250 as reported in [6]. A possible reason is that the spectral phase of the low-order harmonics in our composition (in particular of the 7th) exhibit larger deviations than the one predicted assuming quadratic phase dependence and the measured values for the harmonic chirp Δt [42]. Another factor is the intensity dependence of the temporal drift $\Delta t \propto 1/I_{\mathrm{L}}$ [6] resulting in a spectral phase variation within the laser pulse envelope. In addition to the temporal variation, the spatial intensity variation at the laser focus is found to play an even more important role. Whether the observed deviation from the FTL value is due to

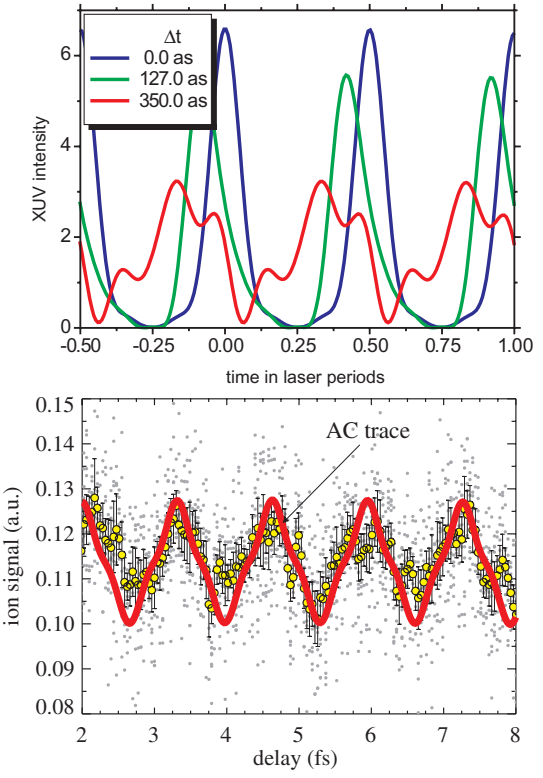

Figure 10. The effect of the harmonic chirp. *Top panel:* the intensity of the superposition of the five harmonics with relative intensity ratios 0.32(7th):1.0(9th):0.30(11th): 0.11(13th):0.01(15th) for a phase spectral difference $\Delta t = 0$, 127 and 350 as. The pulse duration in this case is 315 as. *Lower panel:* comparison of the experimental AC to the collinear AC trace of the pulse train with $\Delta t = 350$ as.

temporal or spatial harmonic phase variation cannot be inferred from these measurements.

The method employed of direct second-order XUV autocorrelation makes perceptible how precarious it is to infer pulse durations indirectly from partial knowledge of some of the parameters involved. However, the method described here can be used to perform detailed parametric studies under various settings and thus optimize the phase-locking conditions. Moreover, it can be refined to include a second-order frequency resolved XUV gating by employing energy resolved photoelectron detection [43], a full temporal characterization method analogous to the frequency resolved optical gating (FROG). These improvements, complementary to the cross-correlation SPIDER [44, 45] or FROG type [46] approaches, will constitute a crucial step in the quest for ever-shorter well-characterized and intense light pulses thus providing the potential for scientific advances in the field of attoscience.

Acknowledgments

The experiment was performed using the ATLAS laser facility at the Max-Planck-Institut für Quantenoptik, Garching. This work is supported in

part by the European Community's Human Potential Programme under contract CT-HPRN-2000-00133 (ATTO) and the Ultraviolet Laser Facility (ULF) (contract no. HPRI-1999-CT-00074).

References

[1] Hänsch, T. W., 1990, *Opt. Commun.*, **80,** 71.
[2] Farkas, Gy, and Tóth, Cs, 1992, *Phys. Lett.* A, **168,** 447.
[3] Harris, S. E., Macklin, J. J., and Hänsch, T. W., 1993, *Opt. Commun.*, **100,** 487.
[4] Papadogiannis, N. A., Witzel, B., Kalpouzos, C., and Charalambidis, D., 1999, *Phys. Rev. Lett.*, **83,** 4289.
[5] Paul, P. M., Toma, E. S., Breger, P., Mullot, G., Augé, F., Balcou, P., Muller, H. G., and Agostini, P., 2001, *Science*, **292,** 1689.
[6] Mairesse, Y., de Bohan, A., Frasinski, L. J., Merdji, H., Dinu, L. C., Monchicourt, P., Breger, P., Kovaèev, M., Taieb, R., Carré, B., Muller, H. G., Agostini, P., and Salières, P., 2003, *Science*, **302,** 1540.
[7] Tzallas, P., Charalambidis, D., Papadogiannis, N. A., Witte, K., and Tsakiris, G. D., 2003, *Nature*, **426,** 267.
[8] Christov, I. P., Murnane, M. M., and Kapteyn, 1997, *Phys. Rev. Lett.*, **78,** 1251.
[9] Brabec, T., and Krausz, F., 2000, *Rev. mod. Phys.*, **72,** 545.
[10] Hentschel, M., Kienberger, R., Spielmann, C., Reider, G. A., Milosevic, N., Brabec, T., Corkum, P., Heinzmann, U., Drescher, M., and Krausz, F., 2001, *Nature*, **414,** 509.
[11] Kienberger, R., Hentschel, M., Uiberacker, M., Spielmann, C., Kitzler, M., Scrinzi, A., Wieland, M., Westerwalbesloh, T., Kleineberg, U., Heinzmann, U., Drescher, M., and Krausz, F., 2002, *Science*, **297,** 1144.
[12] Kienberger, R., Goulielmakis, E., Uiberacker, M., Baltuska, A., Yakovlev, V., Bammer, F., Scrinzi, A., Westerwalbesloh, T., Kleineberg, U., Heinzmann, U., Drescher, M., and Krausz, F., 2004, *Nature*, **427,** 817.
[13] Corkum, P. B., 1993, *Phys. Rev. Lett.*, **71,** 1994.
[14] Lewenstein, M., Balcou, Ph, Ivanov, M. Yu., L'Huillier, A., and Corkum, P. B., 1994, *Phys. Rev.* A, **49,** 2117.
[15] Baltuška, A., Wei, Z., Pshenichnikov, M. S., Wiersma, D. A., and Szipocs, R., 1997, *Appl. Phys.* B, **65,** 175.
[16] Nisoli, M., Stagira, S., De Silvestri, S., Svelto, O., Sartania, S., Cheng, Z., Lenzner, M., Spielmann, C., and Krausz, F., 1997, *Appl. Phys.* B, **65,** 189.
[17] Morgner, U., Kärtner, F. X., Cho, S. H., Chen, Y., Haus, H. A., Fujimoto, J. G., and Ippen, E. P., 1999, *Optics Lett.*, **24,** 411.
[18] Sutter, D. H., Steinmeyer, G., Gallmann, L., Matuschek, N., Morier-Genoud, F., Keller, U., Scheuer, V., Angelow, G., and Tschudi, T., 1999, *Optics Lett.*, **24,** 631.
[19] Shirakawa, A., Sakane, I., Takasaka, M., and Kobayashi, T., 1999, *Appl. Phys. Lett.*, **74,** 2268.
[20] Drescher, M., Hentschel, M., Kienberger, R., Ulberacker, M., Yakovlev, V., Scrinzi, A., Westerwalbesloh, T., Kleineberg, U., Heinzmann, U., and Krausz, F., 2002, *Nature*, **419,** 803.
[21] Paulus, G. G., Grasbon, F., Walther, H., Villoresi, P., Nisoli, M., Stagira, S., Priori, E., and De Silvestri, S., 2001, *Nature*, **414,** 182.
[22] Jones, D. J., Diddams, S. A., Ranka, J. K., Stentz, A., Windeler, R. S., Hall, J. L., and Cundiff, S. T., 2000, *Science*, **288,** 635.
[23] Baltuška, A., Udem, T., Uiberacker, M., Hentschel, M., Goulielmakis, E., Gohle, C., Holzwarth, R., Yakovlev, V. S., Scrinzl, A., Hansch, T. W., and Krausz, F., 2003, *Nature*, **421,** 611.
[24] Antoine, P., L'Huillier, A., and Lewenstein, M., 1996, *Phys. Rev. Lett.*, **77,** 1234.
[25] Bellini, M., Lyngå, C., Tozzi, A., Gaarde, M. B., Hänsch, T. W., L'Huillier, A., and Wahlström, C.-G., 1998, *Phys. Rev. Lett.*, **81,** 297.

[26] Tzallas, P., Witte, K., Tsakiris, G. D., Papadogiannis, N. A., and Charalambidis, D., 2004, *Appl. Phys.* A, **79**, 1673.
[27] Kobayashi, Y., Sekikawa, T., Nabekawa, Y., and Watanabe, S., 1998, *Optics Lett.*, **23,** 64.
[28] Kobayashi, Y., Ohno, T., Sekikawa, T., Nabekawa, Y., and Watanabe, S., 2000, *Appl. Phys.* B, **70,** 389.
[29] Papadogiannis, N. A., Nersisyan, G., Goulielmakis, E., Rakitzis, T. P., Hertz, E., Charalambidis, D., Tsakiris, G. D., and Witte, K., 2002, *Optics Lett.*, **27,** 1561.
[30] Wabnitz, H., Bittner, L., de Castro, A. R. B., Döhrmann, R., Gürtler, P., Laarmann, T., Laasch, W., Schulz, J., Swiderski, A., von Haeften, K., Möller, T., Faatz, B., Fateev, A., Feldhaus, J., Gerth, C., Hahn, U., Saldin, E., Schneidmiller, E., Sytchev, K., Tiedtke, K., Treusch, R., and Yurkov, M., 2002, *Nature*, **420,** 482.
[31] Papadogiannis, N. A., Nikolopoulos, L. A. A., Charalambidis, D., Tzallas, P., Tsakiris, G. D., and Witte, K., 2003, *Phys. Rev. Lett.*, **90,** 133902; Papadogiannis, N. A., Nikolopoulos, L. A. A., Charalambidis, D., Tsakiris, G. D., Tzallas, P., and Witte, K., 2003, *Appl. Phys.* B, **76,** 721.
[32] Peatross, J., Chaloupka, J. L., and Meyerhofer, D. D., 1994, *Optics Lett.*, **19,** 942.
[33] Gaarde, M. B., and Schafer, K. J., 2002, *Phys. Rev. Lett.*, **89,** 213901.
[34] Constant, E., Mével, E., Zaÿr, A., Bagnoud, V., and Salin, 2001, *J. Phys.* IV (France), **11,** Pr2-537.
[35] Mashiko, H., Suda, A., and Midorikawa, K., 2003, *Appl. Phys.* B, **76,** 525.
[36] Durfee, C. G., Backus, S., Kapteyn, H. C., and Murnane, M. M., 1999, *Optics Lett.*, **24,** 687.
[37] Altucci, C., Beneduce, C., Bruzzese, R., de Lisio, C., Sorrentino, G. S., Starczewski, T., and Vigilante, F., 1996, *J. Phys.* D: *Appl. Phys.*, **29,** 68.
[38] Hergott, J. F., Kovacev, M., Merdji, H., Hubert, C., Mairesse, Y., Jean, E., Breger, P., Agostini, P., Carré, B., and Salières, P., 2002, *Phys. Rev.* A, **66,** 021801(R).
[39] Le Deroff, L., Salières, P., and Carré, B., 1998, *Optics Lett.*, **23,** 1544.
[40] L'Huillier, A., Balcou, P., Candel, S., Schafer, K. J., and Kulander, K. C., 1992, *Phys. Rev.* A, **46,** 2778.
[41] Cheng, Z., Furbach, A., Sartania, S., Lenzner, M., Spielmann, C., and Krausz, F., 1999, *Optics Lett.*, **24,** 247.
[42] Salières, P., 2004, personal communication.
[43] Sekikawa, T., Katsura, T., Miura, S., and Watanabe, S., 2002, *Phys. Rev. Lett.*, **88,** 193902.
[44] Muller, H. G., 2002, *Appl. Phys.* B, **74** (Suppl.), S17.
[45] Quéré, F., Itatani, J., Yudin, G. L., and Corkum, P. B., 2003, *Phys. Rev. Lett.*, **90,** 073902.
[46] Norin, J., Mauritsson, J., Johansson, A., Raarup, M. K., Buil, S., Persson, A., Dühr, O., Gaarde, M. B., Schafer, K. J., Keller, U., Wahlström, C.-G., and L'Huillier, A., 2002 *Phys. Rev. Lett.*, **88,** 193901.